Polyvinylpyrrolidone Facilitates Formation of {111}-faceted Au Nanocrystals: Insights from Density-Functional Theory and Molecular Dynamics

S.-H. Liu[*], W. A. Saidi[***], Y. Zhou[*], and K. A. Fichthorn[*,**]

[*]Department of Chemical Engineering, and [**]Department of Physics,
The Pennsylvania State University, University Park, PA, United States, fichthorn@psu.edu
[***]Department of Mechanical Engineering and Materials Science,
University of Pittsburgh, Pittsburgh, PA, United States

ABSTRACT

We use dispersion-corrected density-functional theory (DFT) and classical molecular dynamics (MD) to resolve the role of polyvinylpyrrolidone (PVP) in the shape-selective synthesis of {111}-faceted Au nanostructures. Using DFT, we investigate the adsorption-induced surface energies and spatially-resolved binding of PVP monomer analogs on Au(111), Au(100), and (5 x 1) Au(100)-hex. The calculations indicate that {111} facets would be favored in Au nanostructures grown with the help of PVP. Using MD simulations based on an *ad hoc* interatomic potential fitted to our DFT results, we probe the PVP-induced surface energies, PVP binding affinities, and oxygen density profile of atactic PVP icosamers on Au(111) and (5 x 1) Au(100)-hex. From the DFT and MD studies, we conclude that {111}-faceted Au nanocrystals are preferred in PVP-mediated synthesis, consistent with experiment. The reconstruction of Au(100) is important in achieving {111} facet selectivity.

Keywords: polyvinylpyrrolidone, nanostructures, reconstruction, density-functional theory, molecular dynamics

1 INTRODUCTION

Metal nanocrystals (*e.g.*, Au, Pt, Ag, and Pd) are of key interest for applications in catalysis, sensing, and solar cells, where the nanocrystal size and shape, controlled by structure-directing agents (SDA) in the solution-phase synthesis, can significantly affect its properties. Therefore, it is important to achieve controlled syntheses of these metal nanocrystals.

Polyvinylpyrrolidone (PVP) is a widely used SDA for the shape-selective synthesis of these metal nanostructures. PVP tends to promote {100}-faceted Ag nanostructures and {111}-faceted Au nanostructures. For example, {100}-faceted Ag nanocrystals, such as nanowires and nanocubes [1], are observed in PVP-mediated syntheses. However, {111}-faceted Au nanocrystals, such as nanotetrahedra and nanoicosahedra [2], occur in experiment. These differences are interesting as Ag and Au are isoelectronic with nearly the same lattice constant.

It is hypothesized that PVP binds more strongly to certain crystal facets, which are the most prevalent ones in the metal nanostructures. Because it is difficult to directly measure the binding-energy differences with experiments, atomic-scale theoretical methods such as density-functional theory (DFT) have great potential to resolve facet-selective binding. We recently used dispersion-corrected DFT to show that the repeat unit of PVP has stronger binding to Ag(100) than Ag(111), leading to {100}-faceted Ag nanostructures [3]. We further used our DFT results to fit an empirical force field for the binding of PVP on Ag surfaces. Molecular dynamics (MD) simulations using this force field showed that PVP decamers bind more strongly to Ag(100) than Ag(111) [4].

As we investigate the origins of {111} facet selectivity for PVP on Au using the similar approach as we did for PVP on Ag, it is important to recognize that the Au(100) surface is likely to exhibit a quasi-hexagonal reconstructions [5]. The (5 x 1) hexagonal reconstruction on Au(100) is considered in this study as a model for the (5 x N) family that has been experimentally observed [6]. We resolve PVP binding on Au(111), Au(100), and (5 x 1) Au(100)-hex at the segment level using dispersion-corrected DFT and at the chain level using classical MD.

2 DFT STUDIES OF PVP MONOMER ANALOGS

2.1 Methods

To model the binding of PVP on Au surfaces using DFT, we considered the interaction of 2-pyrrolidone (2P) (*cf.*, Fig. 1) with Au slabs. Experimental studies suggest that PVP binds to Au surfaces via the oxygen in the 2P ring [7], so 2P is likely to be the most active group in the repeat unit of the PVP polymer. Three possible Au surfaces that could occur are considered in DFT: Au(111), Au(100), and (5 x 1) Au(100)-hex (*cf.*, Fig. 1).

Our DFT calculations were performed with the Vienna *Ab Initio* Simulation Package (VASP) [8-10], employing projector augmented-wave (PAW) pseudopotentials [11] to describe electron-nucleus interactions, and the generalized-gradient approximation (GGA) exchange-correlation functional by Perdew, Burke, and Ernzerhof (PBE) [12].

Long-range van der Waals (vdW) interactions are included with the PBE+vdW^{surf} method [13-15]. Other details of these calculations are described in our work [16].

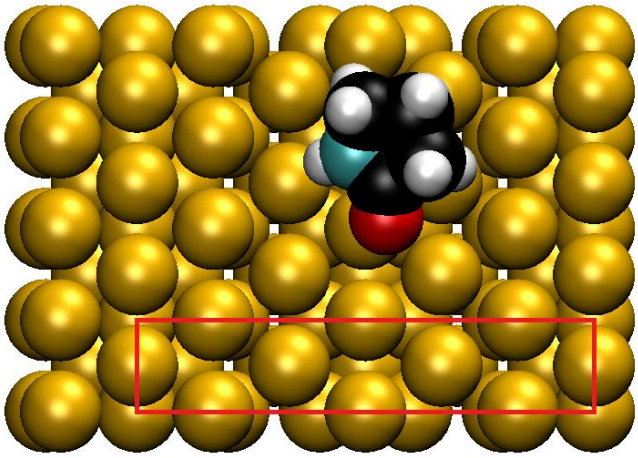

Figure 1: Top-down view of one 2P binding conformation on (5 x 1) Au(100)-hex. Oxygen is red, nitrogen is blue, carbon is black, and hydrogen is white. The red rectangle shows the (5 x 1) unit cell of Au(100)-hex.

2.2 2P Binding Sites and Energies

We built initial 2P structures where the oxygen atom is near to the high-symmetry sites on each of the Au surfaces. After geometry optimization, the oxygen atom of 2P is the closest atom in 2P to the Au surface, and the 2P ring is slightly tilted away from the Au surface plane, consistent with experimental studies [17].

We computed binding energies (E_{bind}) of 2P to Au using

$$E_{bind} = E_{2P} + E_{Au} - E_{2P+Au}\ , \qquad (1)$$

where E_{2P} is the energy of the optimized 2P in gas phase, E_{Au} is the energy of the optimized bare Au slab, and E_{2P+Au} is the energy of the optimized 2P/Au system. Table 1 shows the range of E_{bind} for all the optimized 2P conformations on the three Au surfaces. It can be seen that the binding energies on Au(111) are fairly similar, while the binding energies on Au(100) and (5 x 1) Au(100)-hex show a greater variation.

	Au(111)	Au(100)	(5 x 1) Au(100)-hex
E_{bind} (eV)	1.01-1.05	0.95-1.12	0.94-1.13
γ_{Au} (eV/Å^2)	0.044	0.054	0.050
$\gamma_{2P,Au}$ (eV/Å^2)	0.036	0.046-0.047	0.043-0.044

Table 1: DFT-calculated quantities for Au(111), Au(100), and (5 x 1) Au(100)-hex described in the text.

To obtain further information on how PVP binds to the Au surfaces, we mapped the binding sites of the oxygen atoms in all the optimized 2P conformations. The maps are shown for Au(111), Au(100), and (5 x 1) Au(100)-hex in Figs. 2(a), 2(b), and 2(c), respectively. These binding sites reflect the symmetries of the underlying surfaces. For the purpose of discussion, binding energies below 1.0 eV, between 1.0 and 1.06 eV, and higher than 1.06 eV, are designated as "low", "medium", and "high", respectively.

Figure 2(a) shows that on Au(111), there is a high and uniform density of oxygen binding sites, all with medium (green) binding energies. It indicates that there are many possible ways for PVP to adsorb on Au(111) that lead to similar macromolecular binding energies. On Au(100) shown in Fig. 2(b), the distribution of binding energies is broader than on Au(111). We can see in Fig. 2(b) that one of the sites on Au(100) has a higher binding energy than any site on Au(111), but the rest of the sites have lower binding energies than any site on Au(111).

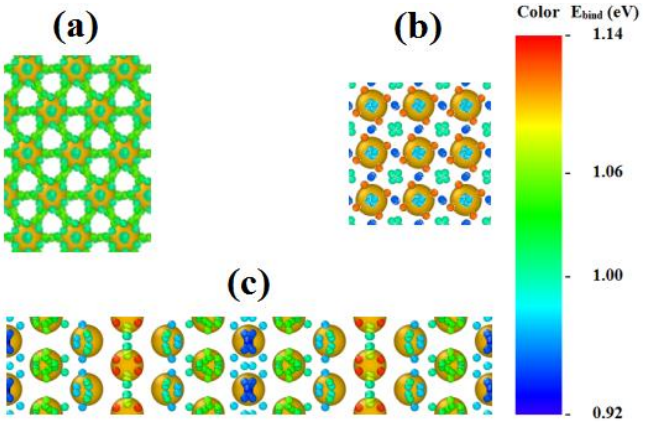

Figure 2: The binding sites for the oxygen atoms of 2P on (a) Au(111), (b) Au(100), and (c) (5 x 1) Au(100)-hex. The binding sites are colored according to their binding energies, indicated by the legend.

Figure 2(c) shows the map for (5 x 1) Au(100)-hex, which indicates that the oxygen binding sites form stripes of binding energies with the repeating pattern: high - low - medium - low - medium - low. From Figs. 2(a) and 2(c), we can see that for (5 x 1) Au(100)-hex, all the binding energies higher than Au(111) are located only in the high-energy stripe. It suggests that PVP binding to the high-energy sites is limited on (5 x 1) Au(100)-hex. Therefore, if there is sufficient coverage of PVP on the (5 x 1) Au(100)-hex surface, the energetic heterogeneity of binding sites may lead to overall comparable or lower PVP binding energies than on Au(111).

2.3 2P-Induced Surface Energies of Au

To understand the effect of 2P adsorption on the surface energies of the Au facets, we calculated the surface energies $\gamma_{2P,Au}$ defined as [18]

$$\gamma_{2P,Au} = \frac{(E_{2P+Au} - NE_{bulk}) - E_{2P} - (E_{Au,fix} - NE_{bulk})/2}{A_{surf}}, \quad (2)$$

where N is the number of Au atoms in the slab, E_{bulk} is the bulk energy per Au atom, $E_{Au,fix}$ is the energy of a bare Au slab fixed at the bulk termination, which is the unreconstructed (1 x 1) surface in all cases, and A_{surf} is the surface area of the slab at 2P/Au interface. The range of surface energies for the three bare (γ_{Au}) and 2P-covered ($\gamma_{2P,Au}$) Au facets is shown in Table 1, where we see that the relative energies of the Au surfaces are virtually unchanged by 2P adsorption. This indicates that in the presence of PVP, {111}-faceted Au nanostructures are thermodynamically favorable.

3 MD STUDIES OF PVP

3.1 Methods

To model the binding of PVP on Au surfaces with MD, we developed force fields for PVP on Au(111) and (5 x 1) Au(100)-hex according to our previous procedure [4]. The details of building and testing these force fields, as well as the parameters for describing the interactions between PVP and Au will be published elsewhere [16]. We implemented these force fields within LAMMPS [19,20], employing an embedded-atom method (EAM) potential [21,22] for Au-Au interactions, and a (slightly [4]) modified CHARMM force field [23] for intra- and inter-molecular interactions of PVP. As we will discuss elsewhere [16], binding energies pedicted by our force field are an excellent match to those predicted by DFT.

3.2 PVP Binding Energies

We performed MD simulations of atactic PVP icosamers binding on Au(111) and (5 x 1) Au(100)-hex surfaces. Atactic PVP is considered because this is the typical tacticity of PVP [24]. Our simulations are in the canonical (NVT) ensemble, where we investigate 24 PVP chains on Au at 550 K, a relevant experimental temperature [25]. Further details of the MD simulations and the equilibrated structures of PVP on Au(111) and (5 x 1) Au(100)-hex will be published elsewhere [16].

We calculated the binding energies of PVP on Au(111) and (5 x 1) Au(100)-hex ($E_{bind,MD}$) using

$$E_{bind,MD} = 24\langle E_{PVP}\rangle + E_{Au,EAM} - \langle E_{PVP+Au}\rangle, \quad (3)$$

where $\langle E_{PVP}\rangle$ is the mean potential energy of one PVP in the gas phase, $E_{Au,EAM}$ is the energy of the optimized, bare Au slab, described by EAM potential, and $\langle E_{PVP+Au}\rangle$ is the mean potential energy of PVP on Au surface. Table 3 shows the binding-energy difference between (5 x 1) Au(100)-hex and Au(111) ($\Delta E_{bind,MD}$) per unit surface area is small.

	(5 x 1) Au(100)-hex - Au(111)
$\Delta E_{bind,MD}$ (eV/Å^2)	0.00039±0.00004
$\Delta\gamma_{Au}$ (eV/Å^2)	0.026
$\Delta\gamma_{PVP,Au}$ (eV/Å^2)	0.026±0.00004

Table 3: MD-calculated quantities with standard errors for differences between (5 x 1) Au(100)-hex and Au(111) described in the text, except for $\Delta\gamma_{Au}$, obtained by EAM.

3.3 PVP-Induced Surface Energies of Au

To investigate the effect of PVP adsorption on the surface energies of the Au facets, we calculated the surface energies $\gamma_{PVP,Au}$ defined as [18]

$$\gamma_{PVP,Au} = \frac{(\langle E_{PVP+Au}\rangle - NE_{bulk}) - \langle E_{24PVP}\rangle - (E_{Au,fix} - NE_{bulk})/2}{A_{surf}}, \quad (4)$$

where $\langle E_{24PVP}\rangle$ is the mean potential energy of 24 PVP chains in a system with the same size as PVP on Au, and the rest of the symbols are defined previously except for PVP/Au interface.

Table 3 shows the differences in surface energies between (5 x 1) Au(100)-hex and Au(111) for bare ($\Delta\gamma_{Au}$) and PVP-covered ($\Delta\gamma_{PVP,Au}$) Au facets. Since $\Delta\gamma_{PVP,Au}$ is nearly the same as $\Delta\gamma_{Au}$, our analysis again indicates that {111}-faceted Au nanostructures are thermodynamically favorable in the presence of PVP.

3.4 Oxygen Density Profiles

To further investigate possible mechanisms by which PVP would facilitate {111}-faceted Au nanostructures, we analyzed the oxygen density profiles for equilibrated PVP on Au(111) and (5 x 1) Au(100)-hex. Because each repeat unit of PVP has one oxygen, this can be a measure of PVP segment density. Details of oxygen density definition and calculations are included in our work [16].

Figure 3 shows the oxygen density (ρ_O) as a function of z direction perpendicular to the surface plane. The two oxygen density peaks arise due to the atactic nature of PVP, and both of these peaks are higher for Au(111) than for (5 x 1) Au(100)-hex. The lower density for (5 x 1) Au(100)-hex near the surface indicates that this surface is not as well protected by PVP as Au(111). Therefore, this lower density could be a driving force for a higher Au flux to (5 x 1) Au(100)-hex, leading to more rapid growth of Au(111).

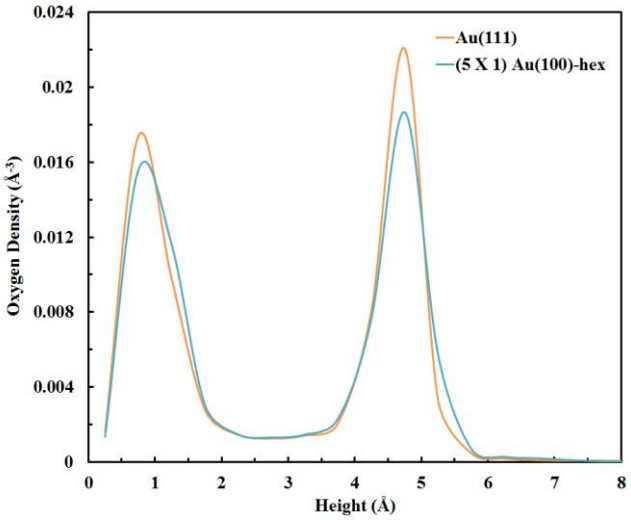

Figure 3: Oxygen density profiles for PVP on Au(111) and (5 x 1) Au(100)-hex.

4 CONCLUSIONS

In summary, we use DFT and MD to resolve the role of PVP in the synthesis of {111}-faceted Au nanostructures. Using DFT, we find that the 2P-covered Au(111) surface is thermodynamically favored. Also, we find that PVP may exhibit a comparable or greater binding affinity for Au(111) than for (5 x 1) Au(100)-hex. Using MD, we find that atactic PVP icosamers have a comparable binding affinity for Au(111) and for (5 x 1) Au(100)-hex and that the PVP-covered Au(111) surface has a lower surface energy than (5 x 1) Au(100)-hex. Further, it is likely that (5 x 1) Au(100)-hex would have a higher Au flux than Au(111). From both thermodynamic and kinetic points of view from DFT and MD, we predict that {111}-faceted Au nanostructures will occur in PVP-mediated synthesis, consistent with experiment. Future studies on characterizing the surface structures of these materials would be useful to achieve shape selectivity.

5 ACKNOWLEDGEMENT

This work was funded by the Department of Energy grant number DE-FG02-07ER46414. This work used the Extreme Science and Engineering Discovery Environment (XSEDE), which is supported by National Science Foundation grant number OCI-1053575.

REFERENCES

[1] Xia, X.; Zeng, J.; Zhang, Q.; Moran, C. H.; Xia, Y. *J. Phys. Chem. C* **2012**, *116*, 21647-21656.
[2] Li, C.; Shuford, K. L.; Park, Q.-H.; Cai, W.; Li, Y.; Lee, E. J.; Cho, S. O. *Angew. Chem.-Int. Edit.* **2007**, *46*, 3264-3268.
[3] Al-Saidi, W. A.; Feng, H.; Fichthorn, K. A. *Nano Lett.* **2012**, *12*, 997-1001.
[4] Zhou, Y.; Saidi, W. A.; Fichthorn, K. A. *J. Phys. Chem. C* **2014**, *118*, 3366-3374.
[5] Fiorentini, V.; Methfessel, M.; Scheffler, M. *Phys. Rev. Lett.* **1993**, *71*, 1051-1054.
[6] Havu, P.; Blum, V.; Havu, V.; Rinke, P.; Scheffler, M. *Phys. Rev. B* **2010**, *82*, 161418.
[7] Mdluli, P. S.; Sosibo, N. M.; Revaprasadu, N.; Karamanis, P.; Leszczynski, J. *J. Mol. Struct.* **2009**, *935*, 32-38.
[8] Kresse, G.; Hafner, J. *Phys. Rev. B* **1993**, *47*, 558-561.
[9] Kresse, G.; Furthmuller, J. *Comput. Mater. Sci.* **1996**, *6*, 15-50.
[10] Kresse, G.; Furthmuller, J. *Phys. Rev. B* **1996**, *54*, 11169-11186.
[11] Blöchl, P. E. *Phys. Rev. B* **1994**, *50*, 17953-17979.
[12] Perdew, J. P.; Burke, K.; Ernzerhof, M. *Phys. Rev. Lett.* **1996**, *77*, 3865-3868.
[13] Tkatchenko, A.; Scheffler, M. *Phys. Rev. Lett.* **2009**, *102*, 073005.
[14] Ruiz, V. G.; Liu, W.; Zojer, E.; Scheffler, M.; Tkatchenko, A. *Phys. Rev. Lett.* **2012**, *108*, 146103.
[15] Al-Saidi, W. A.; Voora, V. K.; Jordan, K. D. *J. Chem. Theory Comput.* **2012**, *8*, 1503-1513.
[16] Liu, S.-H.; Saidi, W. A.; Zhou, Y.; Fichthorn, K. A. (Submitted to *J. Phys. Chem. C*).
[17] Xie, Z. X.; Charlier, J.; Cousty, J. *Surf. Sci.* **2000**, *448*, 201-211.
[18] Zhang, W.; Liu, Y.; Cao, R.; Li, Z.; Zhang, Y.; Tang, Y.; Fan, K. *J. Am. Chem. Soc.* **2008**, *130*, 15581-15588.
[19] Plimpton, S. *J. Comput. Phys.* **1995**, *117*, 1-19.
[20] http://lammps.sandia.gov
[21] Grochola, G.; Russo, S. P.; Snook, I. K. *J. Chem. Phys.* **2005**, *123*, 204719.
[22] http://www.ctcms.nist.gov/potentials
[23] Vanommeslaeghe, K.; Hatcher, E.; Acharya, C.; Kundu, S.; Zhong, S.; Shim, J.; Darian, E.; Guvench, O.; Lopes, P.; Vorobyov, I.; MacKerell, A. D., Jr. *J. Comput. Chem.* **2010**, *31*, 671-690.
[24] Login, R. B. *Kirk-Othmer Encyclopedia of Chemical Technology*; John Wiley & Sons, Inc., 2000; Chapter N-Vinylamide Polymers.
[25] Kim, F.; Connor, S.; Song, H.; Kuykendall, T.; Yang, P. *Angew. Chem.-Int. Edit.* **2004**, *43*, 3673-3677.